RSC Advances

PAPER

View Article Online
View Journal | View Issue

Cite this: *RSC Adv.*, 2021, **11**, 4654

Electrooxidative generation of polymer films from rigid tricarbazole monomers†

Jannis Aron Tent, Robin Ammenhäuser, Marco Braun and Ullrich Scherf *

Received 25th November 2020
Accepted 17th January 2021

DOI: 10.1039/d0ra09988k

rsc.li/rsc-advances

In this report, syntheses and subsequent electropolymerization of a series of five rigid tricarbazole monomers are described. The monomers involve three planar triphenylene-cored tricarbazole-benzenes (with the carbazole units connected *via* their *a*- or *b*-planes) and two triptycene-cored derivatives. Oxidative electropolymerization of these monomers leads to a continuous growth of smooth and freestanding thin films. Moreover, one type of polymer film, based on a poly-*a*-tricarbazole network (**paTC**), shows the occurrence of intrinsic microporosity properties, with a specific BET surface area of 260 $m^2 g^{-1}$.

Introduction

Over the last decades, the interest in developing and improving organic electroactive materials for electronic devices, like organic light emitting diodes, solar cells, or field effect transistors, has been continuously growing.[1] In this regard, the optimization of charge transport properties is one of the primary research goals.[2] Carbazole-derived oligomeric or polymeric materials are often characterized by the occurrence of reversible redox processes,[6] leading to good charge transport abilities.[7] They have been utilized as active components of blue light emitting diodes,[3,4] and organic solar cells.[5] The carbazole building block, hereby, offers a wide scope for chemical functionalization towards individually tailored materials for a specified application.[8–10]

Triazatruxene (TAT), a C_3-symmetric, trimeric indole, can also be described as a molecule where three carbazoles share one central benzene ring.[11] TAT itself showed promising hole transporting abilities.[12] Integrated into a polymer network TAT-based materials have been used for the highly sensitive detection of electron -rich or -poor aromatic systems,[13] as well as for energy storage.[14] TAT-based polymer networks have been synthesized in metal-catalysed reactions, for example oxidative couplings with iron(III)chloride,[15] or Yamamoto-type homocouplings.[13] For the latter, the introduction of additional halogen functions is necessary.[16] Moreover, a proper processing of the resulting unsoluble and intractable polymer powders for further use in electronic devices is challenging.[13] Electropolymerization is a suitable tool to circumvent these processing-related shortcomings since the polymer films are obtained during the synthesis: synthesis and shaping are directly coupled.[17] Following the process of the electrochemical, oxidative coupling of carbazole derivatives in their reactive 3,6-positions, established by Ambrose and Nelson,[6] also carbazole-based polymer networks can be easily produced on a conducting electrode.[18] However, an electropolymerization of TAT as simplest tricarbazole monomer is not possible since the electrogenerated positive charge is localized and stabilized mainly in the electron-rich central benzene ring of the TAT-system.[19] According to the literature, the charge localization in the central ring prevents the coupling between two carbazole units.[19] Thus, we decided to design monomers with an expanded central segment.

In this study, three planar tricarbazole derivatives with an expanded, central triphenylene core are synthesized for the first time, and used for the electrooxidative polymerization into thin films. In addition, two other, rigid tricarbazole derivatives with a triptycene core, first described in a patent of Buchwald *et al.*,[20] are also used for electrochemical thin film generation (Fig. 1). Oxidative coupling and film forming process are investigated by cyclovoltammetry, and with the electrochemical quartz crystal microbalance (EQCM) method. In the case of the **paTC** network, the electropolymerization leads to the formation of thin films of intrinsic microporosity, as so-called microporous polymer networks (MPN).

Results and discussion

The general synthesis route for the three triphenylene-cored, planar tricarbazole derivatives **aTC**, **bTC**, and **bTCu** is described in Scheme 1. Synthetic details and characterization data can be found in the ESI.†

12,19-Dihydro-5*H*-benzo[1,2-*a* : 3,4-*a*′ : 5,6-*a*″]tricarbazole (**aTC**), 12,19-dihydro-5*H*-benzo[1,2-*b* : 3,4-*b*′ : 5,6-*b*″]tricarbazole (**bTC**) and 8,15-dihydro-5*H*-benzo[1,2-*b* : 3,4-*b*′ : 6,5-*b*″]

Bergische Universität Wuppertal, Macromolecular Chemistry Group, Wuppertal Center for Smart Materials and Systems CM@S, Gauss-Str. 20, D-42119 Wuppertal, Germany. E-mail: scherf@uni-wuppertal.de

† Electronic supplementary information (ESI) available. See DOI: 10.1039/d0ra09988k

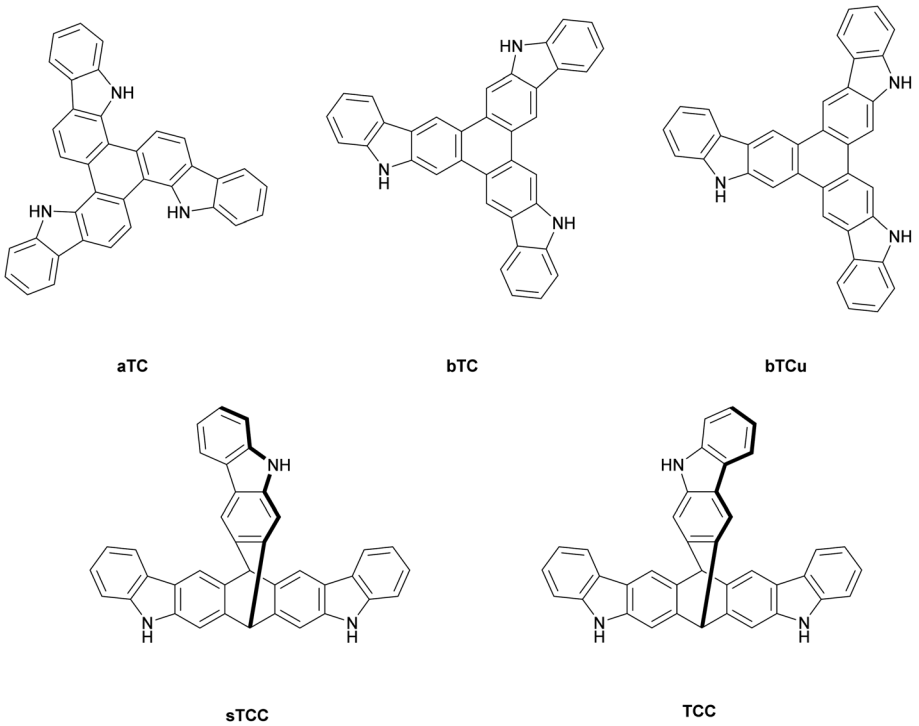

Fig. 1 Chemical structures of the tricarbazole monomers of this study.

tricarbazole (**bTCu**) were synthesized in four steps. After trimerization of the corresponding 1,2-dihalonitrobenzenes into the trinitrotriphenylenes **2** *via* Ullmann couplings, subsequent hydrogenation resulted in the isomeric triamines **3**.[21] Arylation with 1-bromo-2-chlorobenzene with the DavePhos catalyst leads to the secondary tris(diaryl)amines **4**.[20] Finally, a threefold

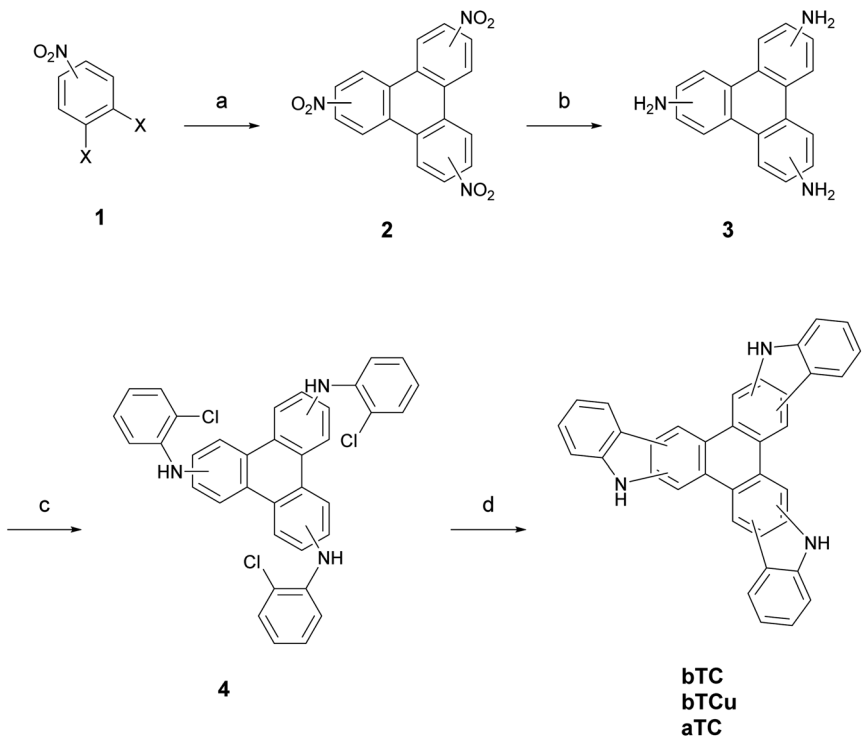

Scheme 1 General synthetic pathway towards the planar tricarbazole derivatives. (a) Cu, DMF, 200 °C, 12 h; (b) H_2, Pd/C, ethyl acetate/ethanol (10/1); (c) *t*-BuONa, 1-bromo-2-chlorobenzene, DavePhos-catalyst, 1,4-dioxane, 125 °C, 18 h; (d) DBU, $Pd(OAc)_2$, $P(t\text{-}Bu)_3$, *o*-xylene, 140 °C, 18 h. (X = Br or Cl).

cyclization (as so-called direct arylation reaction) yielded the tricarbazole monomers.[22] The separation of regioisomeric products is carried out at different stages of the synthesis pathway. For **aTC** synthesis (the carbazole units are condensed *via* their *a*-planes) the separation of the regioisomers is done in step 1, **aTC** is isolated as a light-brownish solid with 53% yield. In contrast, the *b*-connected regioisomeres, the symmetric **bTC** and the non-symmetric **bTCu**, were separated by preparative HPLC after the final reaction step 4. **bTC** was obtained as a light-brownish solid in 5% yield, **bTCu** as a yellow solid in 32% yield. The triptycene-cored monomers were synthesized according to the literature.

Next, the five tricarbazole monomers were polymerized in an electrochemical, oxidative coupling regime, under formation of a polymer network with dimeric dicarbazole connector units. Here, we used different concentrations of the monomers in dichloromethane or acetonitrile in combination with tetrabutylammonium hexafluorophosphate as supporting electrolyte, all in a conventional three electrode cell configuration. The suited potential ranges were first determined for each monomer on a Pt-disc electrode. Film growth and film stability were characterized with the EQCM method. Preparative-scale film generation was performed on ITO-coated glass electrodes (further details are reported in the ESI†). Because all five different monomers showed quite similar behavior in the course of the electropolymerizations, the coupling method will be now discussed exemplarily for the **aTC** monomer. The polymerization of the other monomers is described in the ESI.†

Fig. 2 shows cyclovoltammograms for several oxidative electropolymerization cycles of **aTC** on a Pt-disc electrode. A continuously increasing current during multiple cycles reflects

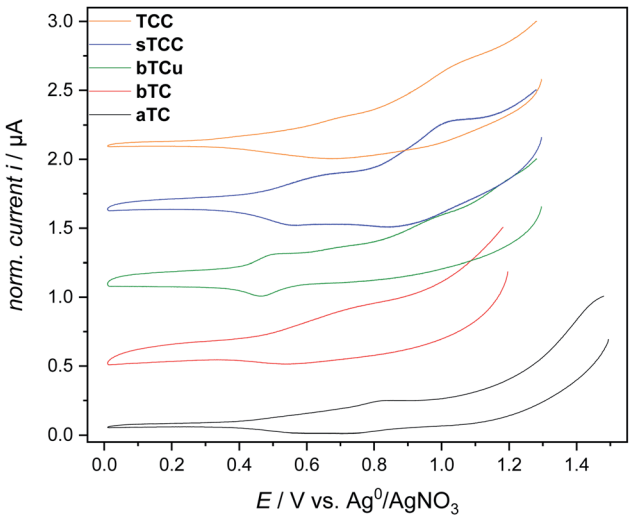

Fig. 3 First cycle cyclovoltammograms for the five tricarbazole monomers, plotted for normalized peak currents. The plots are shifted along the ordinate.

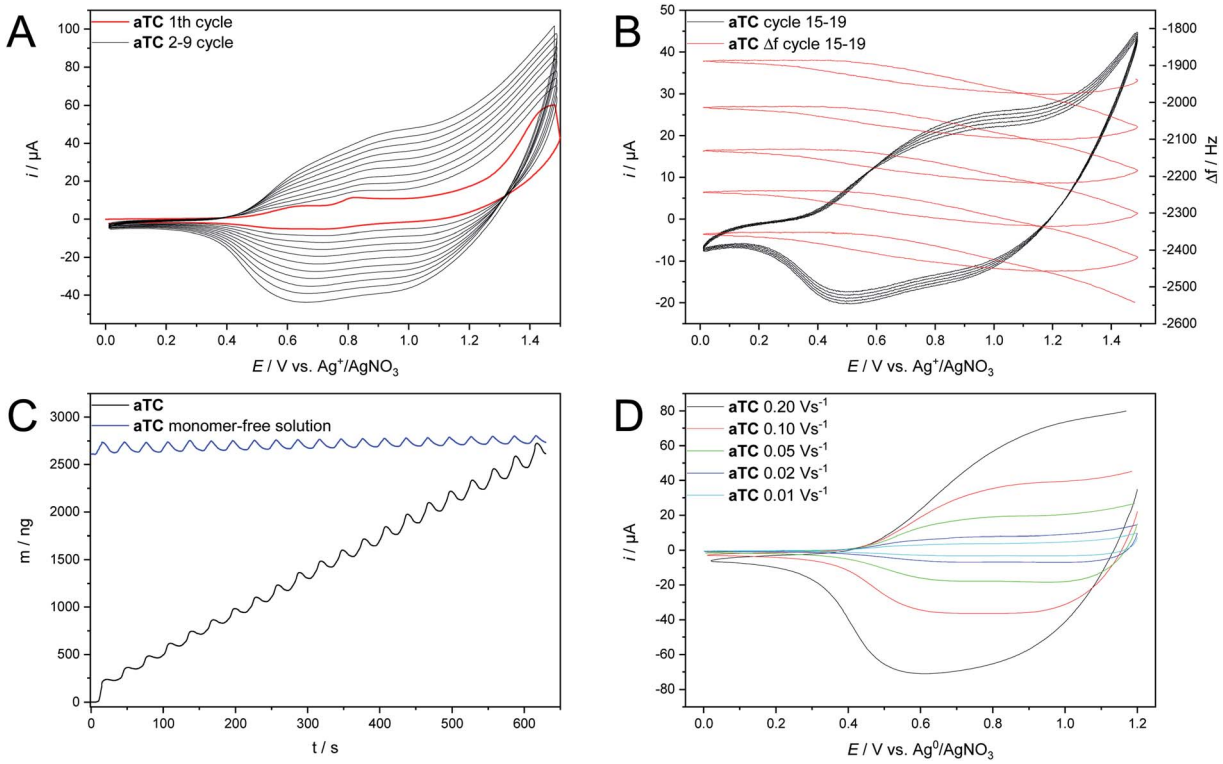

Fig. 2 Electropolymerization of **aTC**. (A) Cyclovoltammograms at a Pt-disc electrode, monomer concentration: $c = 1$ mM in DCM, supporting electrolyte: $TBAPF_6$, potential range: 0–1.5 V, scan rate: 0.1 V s^{-1}, (B and C) EQCM measurements, monomer concentration: $c = 1$ mM in DCM, supporting electrolyte: $TBAPF_6$, potential range: 0–1.5 V, scan rate: 0.1 V s^{-1}, (D) cyclovoltammetric stability tests for **paTC** films, Pt-disc electrode, different scan rates in monomer-free solution, supporting electrolyte: $TBAPF_6$.

Table 1 Energy levels of the tricarbazole monomers and the related polymer films (produced on Pt-electrodes)

	E^{el}_{HOMO} [eV]	E^{opt}_{LUMO} [eV]	E^{opt}_{g} [eV]
aTC	−5.23	−2.14	3.09
paTC	−5.21	−3.36	(1.85)
bTC	−5.23	−2.04	3.19
pbTC	−5.29	−2.51	2.78
bTCu	−5.22	−2.10	3.12
pbTCu	−5.06	−2.00	3.06
sTCC	−5.23	−1.63	3.60
psTCC	−5.22	−2.09	3.13
TCC	−5.24	−1.63	3.61
pTCC	−5.38	−2.00	3.38
TAT[27]	−5.03	−1.68	3.35

the growth of the (semi)conductive film on the electrode. Moreover, the EQCM results of Fig. 2B and C shows a continuous growth of the polymer films of increasing mass/thickness. The observed weight oscillations during each cycle indicate doping/dedoping processes accompanied by the incorporation/extrusion of electrolyte anions into the polymer network.[23] The formed polymer film of **paTC** in monomer-free solution shows a constant average mass despite the ongoing doping/dedoping processes over 20 cycles (Fig. 2C). Additional stability measurements of a **paTC** film on a Pt-disc electrode (Fig. 2D) document a nearly linear correlation between peak current and scan rate. These results document the formation of well-adhering deposits of **paTC** on the electrode whereby the electron transfer is not diffusion-controlled.[24]

Compared to the other planar, triphenylene-cored monomers, for polymerization of the **aTC** monomer application of the widest potential range of 0–1.5 V was necessary (Fig. 3). The *b*-plane-connected monomers **bTC** and **bTCu** with half of their diarylamino groups in *para*-position of their terphenyl units as longest *para*-conjugated segments (in contrast to the presence of exclusively *ortho*-positioned diarylamino groups for **aTC**) allow for the application of somewhat reduced potentials in the range of 0–1.3 V, similar to the potential values described for carbazole polymerizations in the literature.[25,26] The oxidative potential range that was applied to the triptycene-cored monomers **TCC** and **sTCC** was the same as used for polymerization of the monomers **bTC** and **bTCu** (0–1.3 V).

The highest occupied molecular orbital (HOMO) levels of the polymer films were estimated from the onset of the lowest potential oxidation wave (correlated to the HOMO of the ferrocene/ferrocenium couple at 4.8 eV) and are listed in Table 1. Hereby, **pTCC** shows the lowest HOMO level at −5.38 eV, and **pbTCu** the highest HOMO level at −5.06 eV. All other polymers exhibit HOMO levels between −5.21 and −5.24 eV. The corresponding LUMO levels (see Table 1) are calculated as the difference between HOMO level and the optical bandgap, derived from the onset of the absorption bands. Electropolymerization generally induces a lowering of the bandgap if compared to the monomer values, caused by the formation of the dimeric dicarbazole connector units. The bandgap obtained for **paTC** (1.83 eV, given in brackets) strongly differs from the other bandgap values (3.06–3.61 eV), and is caused by a permanent p-doping of the film, accompanied by the occurrence of a broad, low-energy absorption band in the UV/Vis spectrum. The electronic decoupling of the carbazole units in the triptycene-cored monomers is the reason for the somewhat increased bandgaps of the corresponding polymers, if compared to the systems based on the planar tricarbazole monomers. Generally, our tricarbazole-based polymer films show lowered HOMO/LUMO energy levels for similar bandgaps, in comparison to the energy levels that are reported for triazatruxene (TAT)-based polymers (Table 1). These electronic properties favor our polymer films for an application as hole transport layers in electronic and optoelectronic devices.[27]

The optical properties of the five monomers are presented in Table 2 (the spectra are included into the ESI, Fig. 25†). Monomer **aTC** in chloroform solution shows a vibronically structured long wavelength absorption band, with the 0–0 transition as shoulder at *ca.* 417 nm. The corresponding photoluminescence (PL) emission spectrum of **aTC** displays a 0–0 peak maximum at 420 nm, a second maximum at 424 nm, and a shoulder at 463 nm. The very small Stokes shift of *ca.* 3 nm indicates the presence of a rigid, planar chromophore.[28] The adsorption spectrum of polymer network **paTC** displays a absorption maximum at 381 nm and a broad, most probably doping-related long wavelength absorption band in the 400–800 nm region. The **bTC** monomer shows an, in relation to **aTC**, slightly hypsochromically shifted 0–0 absorption shoulder at 387 nm and a weakly structured PL feature peaking at 424 nm (shoulders at 411 and 457 nm). The corresponding **pbTC** polymer film exhibits a broad absorption band with a maximum peaking at 366 nm. The non-symmetric monomer **bTCu** exhibits a long wavelength 0–0 absorption shoulder at 407 nm. The weakly structured emission spectrum displays a PL

Table 2 Optical properties of tricarbazole monomers and corresponding polymer networks

	$\lambda_{max.\ abs.}{}^{a}$ [nm]	$\lambda_{max.\ abs.}{}^{b}$ [nm]	$\lambda_{max.\ abs.}{}^{c}$ [nm]	$\lambda_{max.\ em.}{}^{a}$ [nm]	$\lambda_{max.\ em.}{}^{b}$ [nm]	$\lambda_{max.\ em.}{}^{c}$ [nm]
aTC	331 (359, 389, 417)	381 (499)	296 (381)	435 (420, 463)	—	—
bTC	324 (387)	366	355	424 (411, 457)	—	—
bTCu	312 (336, 357, 407)	302	320 (364, 410)	427 (442)	360 (373, 436)	376 (388, 468)
sTCC	310 (345)	303 (389, 460)	316 (346)	356 (366)	374 (388, 469)	365 (373, 441, 471, 511)
TCC	309 (340)	297 (453)	313 (347)	356 (366, 443, 474, 512)	p (470)	365 (372, 439, 472, 511)

[a] Optical properties of monomer solutions in chloroform. [b] Optical properties of solid monomers on quartz glass. [c] Optical properties of the electropolymerized films.

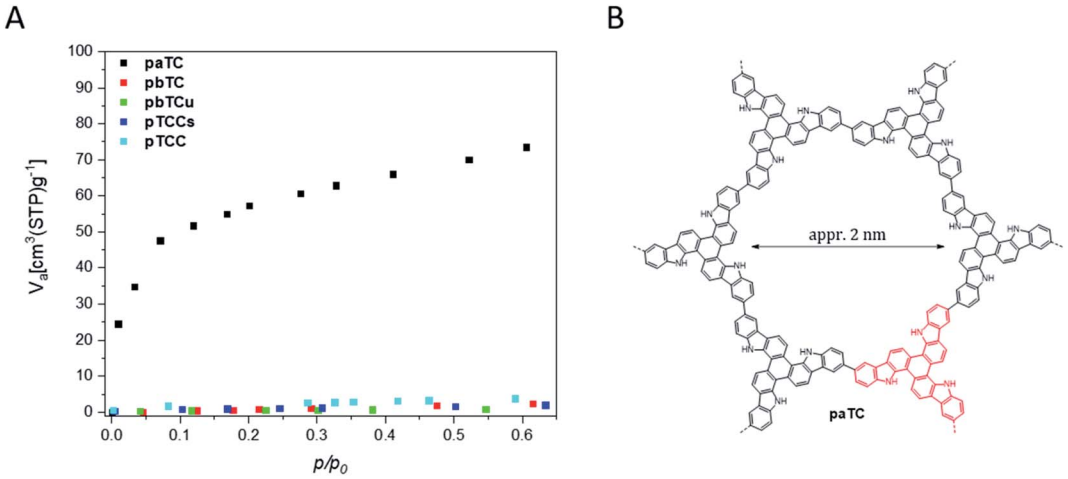

Fig. 4 (A) Krypton gas adsorption isotherms of the electropolymerized films prepared from the tricarbazole monomers. **aTC** (black), **pbTC** (red), **pbTCu** (green), **psTCC** (blue), **pTCC** (cyan). (B) Idealized, hexameric macrocyclic pore of **paTC**.

maximum peaking at 427 nm, that is accompanied by a shoulder at 442 nm. The corresponding polymer network **pbTCu** exhibits a very broad absorption band in the 300–600 nm region with a peak maximum at 302 nm. Both non-planar triptycene-cored monomers show nearly similar optical spectra with 0–0 long wavelength absorption maxima at 345 (**sTCC**) and 340 nm (**TCC**, shoulder), respectively. Both monomers display PL maxima at 356 nm and shoulders at 366 nm. Interestingly, the solid-state luminescence spectra of monomers **TCC** and **sTCC** exhibit low energy features at 443, 474 and 512 nm, that are assigned, based on orienting lifetime measurements, to the occurrence of room temperature phosphorescence. Electropolymerization of the **sTCC** and **TCC** monomers leads to polymer films with broad absorption bands with long wavelength shoulders at *ca.* 460 nm (**psTCC**) and 453 nm (**pTCC**), respectively. The corresponding, weakly structured PL bands of the films peak at 374 nm (**psTCC**, shoulders at 388/469 nm) and 369 nm (**pTCC**, shoulders at 392/470 nm), respectively.

Cyclovoltammetry on ITO-coated glass plates as working electrodes was also used for the preparative generation of thicker films for gas sorption measurements. The thicker films can be easily removed from the electrodes for collecting the needed amount of solid material. The films were collected and washed several times (for the purification procedure see the ESI†), prior to the gas sorption measurements that have been carried out to investigate the (micro)porosity properties of the films. Because of the small amounts of available material, we have used krypton gas adsorption at 77 K and a relative pressure of 0–0.6. For one type of polymer films, for the **paTC** network, a significant and characteristic gas uptake was recorded, as shown in Fig. 4. Because of the fast krypton uptake at low relative pressures (<0.1), the isotherm was categorized as type I according to the IUPAC definitions.[29] Therefore, **paTC** is classified as an inherently microporous polymer network (MPN), with a calculated S_{BET} surface area of *ca.* 260m^2 g^{-1}. NLDFT (nonlocal density functional theory) calculations leads to an average pore diameter of 1.8 nm, a value that is close to the calculated diameter of approximately 2 nm for a pore that is formed in a macrocyclic hexamer unit of **paTC** (see Fig. 4B). The inherent microporosity of the **paTC** films may also explain the observed and already discussed resistant p-doping of the **paTC** polymer films since the micropores are expected to support the incorporation of the respective counter anions into the bulk material.

Table 3 Mean average surface roughness values of the electropolymerized films from tapping mode AFM measurements

	Roughness [nm]	Layer thickness [nm]
paTC	5.8	67–75
pbTC	3.9	58–63
pbTCu	8.0	60–90
psTCC	11.4	46–60
pTCC	14.2	92–126

Tapping mode atomic force microscopy (AFM) analysis of the electropolymerized films from the three triphenylene-cored monomers demonstrate a relatively smooth topology with a mean average roughness of 3.9–8.0 nm at layer thicknesses of 58–90 nm (Table 3). The films made from the two non-planar triptycene-cored monomers show slightly increased mean average roughness values of 11.4/14.2 nm at a layer thickness of 46–60/92–126 nm. All films show the typical cauliflower-like surface topology, characteristic for electrochemically generated polymer networks.[30]

Conclusion

To sum up, three novel, rigid and planar triphenylene-cored tricarbazole monomers, and two, already known, rigid and non-planar triptycene-cored tricarbazoles were synthesized and electrochemically converted into the corresponding polymer

networks, mechanistically as oxidative dimerization of carbazole units. Repetitive carbazole–carbazole couplings lead to a continuous growth of the polymer networks as smooth and freestanding thin films. The polymer films exhibit HOMO energy levels between −5.06 and −5.38 eV, and LUMO energy levels between −2.0 to −2.51 eV, potentially interesting for an application as hole transport layers of (opto)electronic devices. Moreover, one polymeric tricarbazole network (**paTC**) shows the occurrence an intrinsic microporosity with a specific S_{BET} surface area of 260 $m^2 g^{-1}$. A further characterization of the film morphology with wide angle X-ray scattering and transmission electron spectroscopy is planned as well as tests for a potential application of our electropolymerized films as hole transport layers of multilayer electronic devices.

Conflicts of interest

There are no conflicts to declare.

Acknowledgements

We acknowledge support from the Open Access Publication Fund of the University of Wuppertal.

Notes and references

1 X. Guo, M. Baumgarten and K. Müllen, *Prog. Polym. Sci.*, 2013, **38**, 1832.
2 C. Gu, Y. Chen, Z. Zhang, S. Xue, S. Sun, K. Zhang, C. Zhong, H. Zhang, Y. Pan, Y. Lv, Y. Yang, F. Li, S. Zhang, F. Huang and Y. Ma, *Adv. Mater.*, 2013, **25**, 3443.
3 K. Lmimouni, C. Legrand and A. Chapoton, *Synth. Met.*, 1998, **97**, 151.
4 J.-F. Morin, P.-L. Boudreault and M. Leclerc, *Macromol. Rapid Commun.*, 2002, **23**, 1032.
5 T.-Y. Chu, S. Alem, P. G. Verly, S. Wakim, J. Lu, Y. Tao, S. Beaupré, M. Leclerc, F. Bélanger, D. Désilets, S. Rodman, D. Waller and R. Gaudiana, *Appl. Phys. Lett.*, 2009, **95**, 63304.
6 J. F. Ambrose and R. F. Nelson, *J. Electrochem. Soc.*, 1968, **115**, 1159.
7 H. Wang, A. D. Sheikh, Q. Feng, F. Li, Y. Chen, W. Yu, E. Alarousu, C. Ma, M. A. Haque, D. Shi, Z.-S. Wang, O. F. Mohammed, O. M. Bakr and T. Wu, *ACS Photonics*, 2015, **2**, 849.
8 G. Sathiyan, E. K. T. Sivakumar, R. Ganesamoorthy, R. Thangamuthu and P. Sakthivel, *Tetrahedron Lett.*, 2016, **57**, 243.
9 V. Rani and K. S. V. Santhanam, *J. Solid State Electrochem.*, 1998, **2**, 99.
10 J.-F. Morin, M. Leclerc, D. Adès and A. Siove, *Macromol. Rapid Commun.*, 2005, **26**, 761.
11 G. W. Kim, R. Lampande, D. C. Choe, H. W. Bae and J. H. Kwon, *Thin Solid Films*, 2015, **589**, 105.
12 K. Rakstys, A. Abate, M. I. Dar, P. Gao, V. Jankauskas, G. Jacopin, E. Kamarauskas, S. Kazim, S. Ahmad, M. Grätzel and M. K. Nazeeruddin, *J. Am. Chem. Soc.*, 2015, **137**, 16172.
13 X. Liu, Y. Xu and D. Jiang, *J. Am. Chem. Soc.*, 2012, **134**, 8738.
14 X.-C. Li, Y. Zhang, C.-Y. Wang, Y. Wan, W.-Y. Lai, H. Pang and W. Huang, *Chem. Sci.*, 2017, **8**, 2959.
15 A. E. Sadak, E. Karakuş, Y. M. Chumakov, N. A. Dogan and C. T. Yavuz, *ACS Appl. Energy Mater.*, 2020, **3**, 4983.
16 Y.-F. Xie, S.-Y. Ding, J.-M. Liu, W. Wang and Q.-Y. Zheng, *J. Mater. Chem. C*, 2015, **3**, 10066.
17 A. Palma-Cando, D. Woitassek, G. Brunklaus and U. Scherf, *Mater. Chem. Front.*, 2017, **1**, 1118.
18 A. Palma-Cando, E. Preis and U. Scherf, *Macromolecules*, 2016, **49**, 8041.
19 T. G. Thomas, S. Chandra Shekar, R. S. Swathi and K. R. Gopidas, *RSC Adv.*, 2017, **7**, 821.
20 S. L. Buchwald, *US Pat.*, US20140124762 A1, 2014.
21 Y. Li, Y.-X. Wang, X.-K. Ren and L. Chen, *Mater. Chem. Front.*, 2017, **1**, 2599.
22 H. Hagiwara, *JP Pat.*, JP2014169273A, 2014.
23 A. Palma-Cando and U. Scherf, *ACS Appl. Mater. Interfaces*, 2015, **7**, 11127.
24 Y. Wei, C. C. Chan, J. Tian, G. W. Jang and K. F. Hsueh, *Chem. Mater.*, 1991, **3**, 888.
25 V. V. Pavlishchuk and A. W. Addison, *Inorg. Chim. Acta*, 2000, **298**, 97.
26 K. Karon and M. Lapkowski, *J. Solid State Electrochem.*, 2015, **19**, 2601.
27 S. W. Shelton, T. L. Chen, D. E. Barclay and B. Ma, *ACS Appl. Mater. Interfaces*, 2012, **4**, 2534.
28 R. Ammenhäuser, A. Helfer and U. Scherf, *Org. Mater.*, 2020, **02**, 159.
29 K. S. W. Sing, *Pure Appl. Chem.*, 1985, **57**, 603.
30 Y. Xie, *Chem. Rec.*, 2019, **19**, 2370.